**Biogeosciences
Discussions**

Air-sea CO$_2$ fluxes in the Atlantic as measured during the FICARAM cruises

X. A. Padin[1], M. Vázquez-Rodríguez[1], M. Castaño[1], A. Velo[1], F. Alonso-Pérez[1], J. Gago[2], M. Gilcoto[1], M. Álvarez[3], P. C. Pardo[1], M. de la Paz[1], A. F. Ríos[1], and F. F. Pérez[1]

[1]Instituto de Investigaciones Marinas, CSIC, Eduardo Cabello 6, 36208 Vigo, Spain
[2]Instituto Español de Oceanografía (IEO. Vigo), Cabo Estai – Canido, Apartado 1552, 36200 Vigo, Spain
[3]Institut Mediterrani d'Estudis Avançats, CSIC-UIB, Miquel Marqués 21, 07190 Esporles, Spain

Air-sea CO$_2$ fluxes in the Atlantic

X. A. Padin et al.

Title Page

Abstract	Introduction
Conclusions	References
Tables	Figures

|◄ ►|

◄ ►

Back Close

Full Screen / Esc

Printer-friendly Version

Interactive Discussion

Abstract

A total of fourteen hydrographic cruises spanning from 2000 to 2008 were conducted during the spring and autumn seasons between Spain and the Southern Ocean, under the framework of the Spanish research project FICARAM. The performed underway measurements are processed and analysed to describe the meridional air-sea CO$_2$ fluxes (FCO$_2$) along the Atlantic Ocean. The data was organised into different biogeochemical oceanographic provinces, according mainly to the thermohaline characteristics. The obtained spatial and temporal distributions of FCO$_2$ follow the generally expected patterns and annual trends. The Subtropical regions in both hemispheres alternated the CO$_2$ source and sink nature from autumn to spring, respectively. On the other hand, Tropical waters and the Patagonian Sea clearly behaved as sinks of atmospheric CO$_2$ like the waters of the Drake Passage during autumn. The obtained results during the cruises also revealed significant long-term trends, such as the warming of equatorial waters (0.11 ± 0.03°C yr^{-1}) and the decrease of surface salinity (-0.16 ± 0.01 yr^{-1}) in tropical waters caused by the influence of the Amazon River plume. This reduction in surface salinity appears to have a direct influence over the CO$_2$ storage rates, fostering the uptake capacity of atmospheric CO$_2$ (-0.09 ± 0.03 mol m^{-2} yr^{-1}). An analysis of the biogeochemical forcing on the CO$_2$ fugacity (fCO$_2$) variability performed from an empirical algorithm highlighted the major role of the Amazon River input in the tropical North Atlantic fluxes. In addition, it has provided a quantitative measure of the importance of the thermodynamic control of FCO$_2$ at temperate latitudes.

1 Introduction

The CO$_2$ emissions linked with human activity, such as fossil fuel burning, changes in land-use or cement production, have greatly altered the atmospheric CO$_2$ concentrations (Keeling and Whorf, 2000; Houghton, 2003). However, out of the total CO$_2$ released to the atmosphere only half of it ($\sim$9.1 PgC yr^{-1} at present; Canadell et al.,

2007) remains under a stationary storage state in this environmental compartment (Sarmiento and Gruber, 2002; Sabine et al., 2004). In this regard, the oceanic and terrestrial ecosystems play out a major part as they sequestrate a good deal of this greenhouse gas, thus modulating its atmospheric presence and thereby affecting greatly the temperature that is sensed in the biosphere (Siegenthaler and Sarmiento, 1993).

The air-sea CO$_2$ fluxes (FCO$_2$) has lingered over the years as one of the most loosely-tracked and uncertain terms in the carbon system, introducing large uncertainties in global carbon budget estimates, particularly at interannual scales (Keeling et al., 1995; Francey et al., 1995; Battle et al., 2000). This stems from the sparseness and shortage of in situ FCO$_2$ measurements and from the lack of time-series records on a long-term basis. In this context, it is important to strive for a better monitoring of this variable in order to restrain the uncertainties attached to ocean CO$_2$ uptake estimates and to its variability. The coverage of in situ measurements can be largely enhanced through international cooperation research programs and from the use of as much of the available ship-potential as possible. This was the motivation that fostered the Spanish project FICARAM (Air-sea CO$_2$ fluxes along meridional tracks in the Atlantic Ocean), which was born as part of an international effort to carry out extensive measurements that would cover ocean basin scales. More specifically, FICARAM was developed within the framework of larger European projects such as CAVASOO (Carbon Variability Studies by Ships Of Opportunity) and CARBOOCEAN (Marine Carbon Sources and Sinks Assessment). The compendium of datasets generated during FICARAM has been made available from several global databases.

The FICARAM cruises (Table 1) were carried out profiting from courses carried regularly on a six-month basis between Spain and the Antarctic from 2000 to present day, before and after the Antarctic research programme during the austral summer. The underway measurements of surface seawater fugacity of CO$_2$ (fCO$_2^{sw}$) gathered along the tracks of the ships show the variability of this property within different physical-chemical regimes. These repeated measurements aim to provide an in-detail description of the meridional fCO$_2^{sw}$ distributions in the Atlantic (Keeling, 1968; Lefévre, 1997) that will

desirably refine the FCO$_2$ estimates and our knowledge of its long-term trends. The assort of regions sampled during the FICARAM cruises varies from highly productive areas located in upwelling systems to oligotrophic intertropical gyres. The tracks also covered the large areas of the North and South Atlantic Oceans, known to behave as important sinks of atmospheric CO$_2$ at (Takahashi et al., 2008). The aim of the present work is presenting a comprehensive outlook of the fCO$_2^{sw}$ datasets collected during the FICARAM cruises, analyzing the seasonal differences recorded and the interannual variability along the meridional transects in the Atlantic Ocean.

2 Dataset and methods

2.1 The FICARAM cruises

A total of fourteen FICARAM cruises were conducted on board the research vessels B/O Hespérides and B/O Las Palmas beginning in October 2000 until to nowadays (Table 1). While covering approximately the same transit between the southern Spanish and northern Moroccan coasts and the Southern Ocean (Fig. 1), the heading of the courses was southward during boreal falls and northward in boreal springs. The tracks were under military steering and framed within the Antarctic research program for doing maintenance chores and bringing supplies to the Spanish Antarctic bases Gabriel de Castilla and Juan Carlos I, located in the Deception and Livingston Islands, respectively.

The FICARAM cruises mainly sampled the Eastern North and Western South Atlantic basins. Nonetheless, in order to record as faithfully as possible the meridional variability of fCO$_2^{sw}$ it was initially attempted to stick as much as possible to meridian 28° W while underway, but this was normally subject to ship-time availability. Unfortunately, this practice ceased after the FICARAM 9 cruise, when the vessels started operating as ships of opportunity and sailed directly from departure to arrival ports. The FICARAM 6 cruise was another exception that could not sail along the 28° W meridian

for long.

2.2 Equipment installation

The underway measurements of sea-surface and atmospheric molar fractions of CO_2 (xCO_2^{sw} and xCO_2^{atm}, respectively) were performed with a GASPAR apparatus. This autonomous device was fully devised and assembled at Instituto de Investigacións Mariñas (IIM-CSIC, Vigo-Spain), based on a previous setup developed by researchers at the Institut für Meereskunde (Kiel-Germany; Körtzinger et al., 1996). The analytical principle of the GASPAR is based on the equilibration of a carrier gas phase with the seawater parcel under analysis. Subsequently, the CO_2 mixing ratio in the carrier gas is determined with an infrared analyser.

There exist several systems that allow reaching the equilibration between the carrier gas phase and the sample. The equilibrator system of GASPAR combines the advantages of a laminar flow system (Poisson et al., 1993) and a bubble-type system (Takahashi, 1961). The bubble equilibrator is a chamber of 1.5 L volume that is being constantly renewed with incoming seawater, while the laminar flow equilibrator consists of a 30 cm high glass column with two concentric cylinders to provide thermal insulation for the water flow that is centered at the top of the water chamber. A fixed volume of air recirculates through this system at a flow rate of $0.8\,L\,min^{-1}$ and it is virtually in continuous equilibrium with the seawater phase that is being constantly renewed. The system is vented to the atmosphere through an air ballast bottle flushed by an external air stream to the ship for avoiding enriched CO_2 air inputs from the lab. Meanwhile, seawater is being continuously pumped from 3 m under the waterline into the ship's hull at a high flow rate to avoid warming of the seawater sample (1.5 L) prior to entering the apparatus. The atmospheric air is thrusted with an air pump through a Dekabon tube mounted on the windward side of the ship's mast to avoid exhaust fumes from the ship's engine.

The molar fractions of CO_2 and H_2O were measured with a non-dispersive infrared Li-COR analyser (model 6262) which is catalogued as the best-known experimental

practice to determine the partial pressure of CO_2 (pCO_2) in an air-flushing equilibrator (DOE, 1994). This instrument has a reference channel (apart from the measuring channel) where a dry CO_2-free gas is recirculated at a rate of $0.2\,L\,min^{-1}$. Altogether, two standards were used through this channel alternatively, namely, CO_2-free air and a CO_2 standard gas of known concentration (375 ppm) certified by Instituto Meteorológico Nacional de Izaña (Canary Islands, Spain). The different gas streams are passed through the Li-COR via miniature solenoid valves, which were used as selection switches between the different measuring modes, i.e., atmosphere, air from the equilibrator or standard gases. A visual basic software routine allowed for the automation of the system by managing the measuring intervals of each mode. The typical measuring routine configuration consisted of a calibration phase, in which 20 measurements for each of the two gas standards were performed. Immediately after, a routine of 24 uninterrupted cycles of one hour long each (55 min devoted to seawater sample measurements and 5 min for atmospheric air records) is started.

A thermosalinograph (SBE-45-MicroTSG) fed by a bifurcation of the uncontaminated seawater supply was coupled to GASPAR and recorded underway surface temperature (SST) and salinity (SSS) during the B/O Las Palmas cruises. When onboard the B/O Hespérides these data were gathered via the vessel-mounted oceanographic data acquisition system.

2.3 Estimation of air and sea fCO_2 and air-sea CO_2 exchanges

The xCO_2^{atm} values were linearly interpolated versus latitude, using monthly measurements from selected meteorological stations of the NOAA/ESRL Global Monitoring Division located close to ship tracks (Fig. 1), namely: Mace Head (Ireland, 53.33° N), Azores (Portugal, 38.77° N), Izaña (Spain, 28.3° N), Ascension (UK, 7.92° S), Arembepe (Brazil, 12.77° S), Tierra de Fuego (Argentina, 54.87° S) and Palmer Station (US, 64.92° S). This dataset was preferred to the in situ xCO_2^{atm} measurements in most cases, given the lack of ship records during some of the FICARAM cruises. For consistency sake, measurements from the NOAA/ESRL were used in all cases. The afore-

Air-sea CO_2 fluxes in the Atlantic

X. A. Padin et al.

Title Page

Abstract	Introduction
Conclusions	References
Tables	Figures

|◄ | ►|

◄ | ►

Back | Close

Full Screen / Esc

Printer-friendly Version

Interactive Discussion

mentioned interpolation infers negligible random errors in the air-sea flux calculations for the large majority of the seasonal cycle (Padin et al., 2007). The record gaps in the time-series from these stations were completed from a fit between ship measurements and a theoretical curve, which consists of a combination of a seasonal cycle trend with the annual and semi-annual harmonics (Padin et al., 2007). The final xCO_2^{atm} dataset was then converted to pCO_2^{atm} (Eq. 1) and, for this conversion, the partial pressure of water vapour (pH$_2$O, in atm) was calculated from in situ SST (T_{is}, in °C) readings (Cooper et al., 1998) (Eq. 2). Finally, when calculating fCO_2^{atm} from pCO_2^{atm} values, a decrease of 0.3% is considered of acceptable accuracy (Weiss, 1974) while for greater differences the values are flagged.

$$pCO_2^{atm} = xCO_2^{atm}(p^{atm} - pH_2O) \tag{1}$$

$$pH_2O = 0.981\exp(14.32602 - (5306.83/(273.15 + T_{is}))) \tag{2}$$

The measured xCO_2^{sw} data was converted to fCO_2^{sw} referenced to saturated water vapour pressure using the atmospheric pressure readings from the DOE Handbook (1994) compliant barometer installed in the GASPAR system. The fCO_2^{sw} values were then corrected for the seawater temperature shift caused by the passing from the hull's inlet into the equilibration chamber that was usually lower than 1°C. This temperature tracking was done with platinum resistance thermometers and then applying the empirical equation proposed by Takahashi et al. (1993; $\delta\ln pCO_2/\delta T = 0.04231 C^{°-1}$).

$$FCO_2 = a\,k\,S\,\Delta fCO_2 \tag{3}$$

The FCO_2 (mol m^{-2} yr^{-1}) was calculated applying Eq. (3), where "a" is a unit conversion factor, "S" (mol kg^{-1} atm^{-1}) stands for the solubility of CO_2 in seawater (Weiss et al., 1974), "k" (cm h^{-1}) is the CO_2 transfer velocity (Wanninkhof, 1992) and ΔfCO_2 (μatm) is the air-sea fCO_2 gradient (i.e. $fCO_2^{sw} - fCO_2^{atm}$). The coefficient "k" was computed from daily anemometric wind speed records at 10 m above sea-surface

Full Screen / Esc

Printer-friendly Version

Interactive Discussion

from the NCEP/NCAR reanalysis project (Kalnay et al., 1996). Data was accessed via the website of the NOAA-CIRES Climate Diagnostics Center, Boulder, Co, USA (http://www.cdc.noaa.gov/). The $\Delta f\text{CO}_2$ was initially estimated with a 1-min frequency but it was then averaged to 5-min cycles.

In addition remotely sensed chlorophyll-*a* (chl-*a*) was included in the FICARAM dataset as a proxy of photosynthetic activity. Weekly fields of chl-*a*, with a spatial resolution of $9\,\text{km}^2$ were remotely recorded by Sea-viewing Wide Field-of-view Sensor (SeaWIFS) Level 3 (Hooker et al., 1992) and downloaded from http://oceancolor.gsfc. nasa.gov/. The selected satellite records of chl-*a* do not have an exact spatiotemporal match with ship measurements: they were chosen from pixels that were taken within ±4 days (orbital over-passing) of the ship measurement date and found within ±6.3 km off the track of the cruise.

2.4 Biogeochemical oceanographic provinces

The study of the meridional Atlantic $f\text{CO}_2^{\text{sw}}$ has been focused on selected biogeochemical provinces, after the pioneering works on this subject from Longhurst et al. (1995) and Hooker et al. (2000). The FICARAM tracks over the Atlantic Ocean (excluding the Mediterranean basin) were delimited according to average boundaries established from SST-SSS relationships, resulting in the following ten regions (Fig. 1):

Eastern North Atlantic Subtropical Gyre (ENAS; 39° N–27° N) is dominated by the Azores Current (Ríos et al., 1992) that is the northeast component of the North Atlantic Subtropical Gyre.

The *Canary Current* (CC; 27° N–16° N) is also a part of the northern subtropical gyre with a moderate flow characterised by a salinity maximum that demarcates the beginning of the tropics. A coastal upwelling is located in the West African continental margin at these latitudes, and its influence can reach as far as 300 km offshore (Mittelstaedt, 1991).

The *North Equatorial Current* (NEC; 16° N–8° N) region is located amidst the zonal currents of the Equatorial Atlantic. This latitudinal band includes the Guinea Dome

Air-sea CO$_2$ fluxes in the Atlantic

X. A. Padin et al.

province (12° N–8° N) characterized by its seasonal upwelling events that stretch from December to April or May (Barton et al., 2001). Despite this, the underway measurements were not affected by the upwelled waters because the cruises normally sailed too far offshore at these latitudes.

The *North Equatorial Counter Current* province (NECC; 8° N–1° N) features a maximum flow from the easterly current during the Boreal Autumn that fades away almost completely during the winter and early spring (Richardson and Reverdin, 1987). This province is also characterized by a band of low-density waters from the Amazon River with a core at 4° N–5° N (Müller-Karger et al., 1988) with SST values of ~25°C (Emery and Dewar, 1982) and a SSS<35.

The *South Equatorial Current* province (SEC; 1° N–15° S) displays a seasonal forcing with a maximum westward flow during the austral winter in the vicinity of the Equator. The South Equatorial Counter Current (SECC) is weakly present between 7° S–9° S.

The *South Atlantic Tropical Gyre* province (STG; 15° S–31° S) has relatively stable thermohaline properties with a gradual decrease of its SST and SSS values. An important poleward component of the Brazil Current that runs along the South American continental shelf is also included in this region.

The *South American Shelf* province (SAS; 31° S–40° S) is also dominated by the Brazil Current, that extends southward as far as 44° S, but has its most outstanding particularity on the strong influence the Plata river exerts here.

The *South Atlantic Convergence* zone (SAC; 40° S–51° S) is a frontal area where the northward Falkland and southward Brazil currents converge that generate high temperature gradients and large heterogeneity in the concentration fields of several chemical properties.

The *Falkland Current* (FC; 51° S–56° S) is a northward looping excursion of the Circumpolar Current that forms a jet of SST and SSS under 10°C and 34.3, respectively (Bianchi et al., 1993).

The *Drake Passage* region, (DP; 56–66° S) extends from the southernmost tip of South America (56° S) to the northern tip of the Antarctic Peninsula (62° S) that is

dominated by a racing eastward flow of Antarctic Circumpolar Current. The Southern Ocean is characterized by a latitudinal succession of circumpolar frontal structures such as the Subantarctic Front, the Polar Front and the Continental Water Boundary.

In addition to the former division, a depth of 200 m was chosen as a boundary to separate ocean from shelf areas in the African and South American continents (Fig. 1). The CO_2 source-sink changes within the continental shelf with respect to depth were also considered: while the distal shelf normally behaves as a CO_2 sink, the proximal shelf is essentially influenced by continental inputs and non-stratified conditions that favour the outgasing of CO_2 to the atmosphere (Thomas et al., 2004; Padin et al., 2007; Chen and Borges, 2009). Consequently, surface (<50 m) coastal waters that corresponded mainly to harbour areas were excluded from the database. The ETOPO2v2 (USDC, NOAA, NGDC 2006) bathymetry was used for merging depth records using two-dimensional linear interpolation functions of every measurement. After applying all of these selection criteria filters the FICARAM dataset comprised a total of 67 845 observations.

3 Results and discussion

3.1 Thermohaline sea-surface variability

The observed thermohaline distribution of the selected biochemical provinces (Fig. 1) springs directly from the meridional differences in the radiation balance, evaporation-precipitation rates and continental inputs (Fig. 2a, b, e, f). In general, Northern Hemisphere waters were warmer than Southern waters during the boreal autumn while the opposite prevailed during boreal springs (Fig. 2a, e). At a seasonal scale the SST changes are maxima in the subtropical regions (4.3°C and 3.5°C at the ENAS and STG regions, respectively; Table 2). Differently, almost negligible seasonal SST differences were observed in equatorial regions (NECC region; Table 2). Regarding the meridional SSS distribution, it shows an inter-hemispheric symmetry like in the case of SST, but

unlike the latter the seasonal variability appears not be so clearly distinguishable in either hemisphere (Fig. 2b, f).

On a more local scale, the ENAS and CC provinces show an equatorward warming of surface waters (2.7 and 2.4°C during autumn and spring, respectively), parallel to a modest increase in SSS. Interestingly, the coastal upwelling off African coasts, between Cape Blanc (21° N) and Cape Bojador (26° N), was recorded during the autumn seasons of the last cruises, manifested from the cooling and SSS decrease observed in the CC province.

The intense intertropical (23.4° S–23.4° N) precipitation rates cause an inversion in the direct SST-SSS relationship observed in Northern Hemisphere provinces. Moreover, the massive continental discharge contributions from the Amazon River generate a sharp and wide band of minimum SSS values in the NECC province. These low SSS values were especially marked in autumn given the most frequent rain during summer and the intensification of eastward currents (Richardson and McKee, 1984). This autumn intensification of freshwater inputs produced a seasonal SSS difference of 0.5, and the fresher record (33.63) was spotted at 4.3° N during autumn 2008. The warmest waters (28.2±0.6°C) of the Atlantic Ocean are also found in the NECC region (Table 2) in autumn, putting forward the evidence of the aforementioned intertropical inverse SST-SSS correlation. The overall warmest waters were located south, in the SEC province during the spring season (Table 2). An average value of 28.7±0.3°C was reached and an outstanding peak of 29.9°C was recorded at 8.6° S during April 2008.

As in the case of Subtropical waters in the North Hemisphere, a clear poleward decrease of SST and SSS was observed in the STG province (Fig. 2a, b, e, f). This trend is also observed in the southward ocean tracks but with colder and fresher waters of coastal origin. The influence of continental inputs was especially intense in the SAS province, where runoffs from the Plata River rule the SSS distributions. This region is characterised by minimum SSS values that reached troughs of 28.31 and 9.35 in the ocean and the distal shelf areas, respectively, during November 2005, which was the month of maximum discharge (Guerrero et al., 1997).

X. A. Padin et al.

The frontal region formed by the convergence of the warm and saline Brazil Current and the cold and less saline Falkland Current generates the strong thermohaline gradients observed offshore in the northern boundary of the SAC region, especially during autumn (Fig. 2e, f). A sharp southward decrease of SST and SSS ($\sim$6°C and

5 $\sim$2 units, respectively) was found during FICARAM 7 (Fig. 2). Surprisingly, the underway measurements along the Patagonian shelf did not reveal the typical circumpolar convergence structures in these latitudes. The distal shelf in this region was usually occupied by a mixture of waters from the Falkland and Brazilian currents and diluted mainly with freshwater outflows from the Plata River (Gordon, 1989). Additionally, it

10 can be inferred from the seasonal changes observed in estuarine flows from shelf waters of the SAC province that freshwater runoffs and the seasonally dominant wind fields determine the influence of fluvial waters in the Patagonian shelf (Table 2, Fig. 2). Accordingly, the dominant southward winds during the boreal autumn-winter seasons (northward in spring-summer) produced the low SSS values registered during the au-

15 tumn cruises.

Yet another local SSS minimum (average 32.9±0.5) was recorded on the distal shelf of the FC (Fig. 2) during autumn cruises (Table 2). This SSS decrease was driven by the important outflow of low salinity waters from the Magellan Strait (Bianchi et al., 2005) caused by the continental ice melting in the Pacific coast of Tierra de Fuego (Pi-

20 ola and Rivas, 1997). On the contrary, none of either the coastal freshwater influence or the seasonal changes reached oceanic waters (Table 2).

The Southern Ocean waters in the DP province were only sampled four times in November 2007 and 2008. The thermohaline spatial distribution shows clearly the well-known meridional zonation of Antarctic waters. Two regions of rapid SST tran-

25 sition at the Antarctic Circumpolar Current point out the locations of the Subantarctic Front ($\sim$57° S) and the Polar Front (58.7° S), respectively (Fig. 2e). Yet another front, the Continental Water Boundary, could be clearly observed around 62° S from the SSS distribution (Fig. 2f). The proximity of the coastline produced an enhanced onshore salt surplus derived from the brine rejection during the formation of Antarctic ice (Fig. 2).

Alternatively, surface waters close to the Livingston Island were the coldest records of all the FICARAM cruises, with an average temperature of $-0.8\pm0.7^{\circ}$C, which is significantly colder than oceanic waters in this region (average $1.1\pm2.0^{\circ}$C; Table 2). Antarctic waters showed significant interannual variability, with a remarkable 0.8°C warmer and 0.2 salinity units fresher waters during autumn 2008 (Fig. 2e, f).

3.2 Distributions of $\Delta f CO_2$ and $F CO_2$

The $\Delta f CO_2$ variability of the northern provinces (Fig. 1) follows roughly the spring and autumn meridional SST distributions, and has an analogous equatorward trend to that of declining SST seasonal amplitudes (Fig. 2c, g). The largest seasonal $\Delta f CO_2$ variability ($43\,\mu$atm of amplitude) was measured for the ENAS province, while the NECC province showed virtually no variability (max. $2\,\mu$atm differences) (Table 2). The maximum air-sea disequilibria in each province corresponded to the autumn season in the Northern Hemisphere, the highest $\Delta f CO_2$ being $16\pm13\,\mu$atm, in the CC region. On the other hand, the lowest $\Delta f CO_2$ in these latitudes were recorded during the spring season reaching minimum values of $-34\pm12\,\mu$atm in the ENAS region. Strongly undersaturated surface waters were sampled in the cruises conducted closer to the coast, such as the FICARAM 9 and 14 (Fig. 1). The maximum undersaturation was found around 20°N, corresponding to the upwelling system along the Mauritanian coast and its typically associated biologically enhanced CO_2 drawdown. The northeastern Atlantic provinces behaved as a sink of atmospheric CO_2 during the successive spring seasons, with an average $F CO_2$ of -1.8 ± 1.2 and $-1.4\pm1.0\,\mathrm{mol\,m^{-2}\,yr^{-1}}$ in the ENAS and CC, respectively. In spite of behaving as a net sink of $-0.22\,\mathrm{PgC\,yr^{-1}}$ at an annual scale (Takahashi et al., 2008), the CO_2 sink behaviour in these regions swapped to CO_2 source during autumn, yielding average $F CO_2$ values of 0.2 ± 0.4 and $0.6\pm0.5\,\mathrm{mol\,m^{-2}\,yr^{-1}}$.

The tropical Atlantic regions (14° N–14° S) were measured to behave as net CO_2 sources, emitting $0.1\,\mathrm{PgC\,yr^{-1}}$ to the atmosphere (Takahashi et al., 2008). Neverthe-

less, the NEC province did not act as a CO_2 source to the atmosphere in any FICARAM cruises. It remained CO_2 undersaturated ($-17\pm10\,\mu$atm) during the spring cruises and close to equilibrium in autumn (Table 2). This quasi-equilibrium also extended across the NECC province during both seasons, with nearly absent CO_2 exchanges.
5 The equatorial upwelling system in the SEC province was highly supersaturated with CO_2 in both spring and autumn (Fig. 2c, g). An average $\Delta f CO_2$ value of $30\pm11\,\mu$atm during spring exceeded slightly the $24\pm12\,\mu$atm autumn records and caused a subtle shift of released CO_2 between the spring and autumn seasons in this region, from $0.7\pm0.5\,\text{mol m}^{-2}\,\text{yr}^{-1}$ to $1.0\pm0.7\,\text{mol m}^{-2}\,\text{yr}^{-1}$, respectively. Alternatively, the stretch of
10 surface waters acting as a CO_2 source showed important changes at a seasonal scale, and reached even the southern latitudes during autumn season (Fig. 2c, g).

Regarding the Southern Hemisphere, the subtropical waters of the STG province were characterized by a poleward undersaturation increase with respect to the atmosphere, parallel to the SST and SSS decreases (Fig. 2c, g). The estimated $F CO_2$ for
15 open ocean waters revealed an inverse seasonal behaviour to the one observed in the North Atlantic: STG oceanic waters acted as a source of $0.6\pm0.6\,\text{mol C m}^{-2}\,\text{yr}^{-1}$ during spring and as a slight sink of $-0.2\pm0.7\,\text{mol C m}^{-2}\,\text{yr}^{-1}$ in autumn (Table 2). Opposite to the seasonal variability expected for ocean waters, the distal shelf of the STG region behaved as a slight CO_2 source during the spring and autumn seasons
20 ($0.4\pm0.4\,\text{mol m}^{-2}\,\text{yr}^{-1}$ and $0.5\pm0.7\,\text{mol m}^{-2}\,\text{yr}^{-1}$, respectively) (Table 2).

On the contrary, most provinces in the Patagonian Sea acted as an intense CO_2 sink during the autumn and spring seasons, particularly in shelf areas. In general, the estimated $\Delta f CO_2$ and $F CO_2$ distributions match roughly with some recently reported results in the Patagonian Sea by Bianchi et al. (2009). The latter has reported average
25 autumn $\Delta f CO_2$ and $F CO_2$ values of $-67\,\mu$atm and $-2.5\,\text{mol m}^{-2}\,\text{yr}^{-1}$, respectively and $-20\,\mu$atm and $-1.1\,\text{mol m}^{-2}\,\text{yr}^{-1}$ for the spring seasons. Surprisingly, such results are opposite to what could be expected from the observed seasonal shifts of chl-a, which indicate higher photosynthesis activity during warm, more stratified spring conditions. Those results suggest that the intensely enhanced production of chl-a in ocean and

X. A. Padin et al.

shelf waters of the Patagonian Sea from copious nutrient inputs (Bakun and Parrish, 1991) and photosynthetic cell accumulation in frontal regions (Froneman et al., 1999) would not be responsible for the biological CO_2 drawdown. Most of these primary production stimulating mesoscale processes, such as continental runoffs, current interactions and frontal regions produced abrupt changes in the ΔfCO_2 and FCO_2 distribution (Fig. 2c, d, g, h) and set forth the complex hydrography in these regions (Bianchi et al., 2009).

Like the rest of Patagonian provinces, the SAS measurements classify this region as an intense CO_2 sink, especially in the shelf areas during the austral spring (average CO_2 sequestration of $-3.2\pm2.7\,\mathrm{mol\,m^{-2}\,yr^{-1}}$; Table 2). These uptake rates exceeded the air-sea CO_2 exchanges estimated in the SAC province in both spring and autumn. Similarly to Bianchi et al. (2009), ΔfCO_2 values lower than $-190\,\mu\mathrm{atm}$ were measured over the shelf-break waters during the austral spring (Fig. 2g). Notwithstanding the potential of shelf waters, oceanic waters of the SAS province are rated as the strongest CO_2 sink recorded in the FICARAM history (Table 2), with an average uptake rate of $-5.4\pm3.6\,\mathrm{mol\,m^{-2}\,yr^{-1}}$ in average wind speed (WS) fields of $9.9\pm3.1\,\mathrm{m\,s^{-1}}$.

The distal shelf of the FC province also behaved as a particularly intense CO_2 sink ($-1.4\pm3.2\,\mathrm{mol\,m^{-2}\,yr^{-1}}$) during the austral spring. However, oceanic waters of this province showed seasonal shifts in the direction of FCO_2: it went from strong undersaturation states ($-50\pm40\,\mu\mathrm{atm}$) in autumn to equilibrium conditions ($1\pm26\,\mu\mathrm{atm}$) during spring (Table 2). In spite of the latter modest ΔfCO_2 values, the WS fields in this region, one of the world's mightiest (Trenberth et al., 1990) that reached values of $\sim17.6\,\mathrm{m\,s^{-1}}$ during spring 2002, contributed considerably to make this area a notable outgasing zone of $1.2\pm2.5\,\mathrm{mol\,m^{-2}\,yr^{-1}}$.

The autumn ΔfCO_2 measurements in Antarctic waters gathered during two of the FICARAM cruises are in good agreement with the far well documented behaviour of the Southern Ocean as an important sink of atmospheric CO_2 (Metzl et al., 1999), with a marked interannual variability (Metzl, 2004). All records concur in the undersaturation of these waters during the successive autumns and repetition of the in-

5603

terannual variability observed also in the thermohaline field (Fig. 2). The Antarctic average $\Delta f\mathrm{CO}_2$ fields during 2007 were homogeneous and slightly undersaturated ($-10\pm4\,\mu$atm) and increased up to $-21\pm21\,\mu$atm during the following year. In spite of these differences, $\Delta f\mathrm{CO}_2$ values were locally clustered around $-20\,\mu$atm in the vicin-
ity of the Polar Front during both years. South from this latitude, there was a marked southward $\Delta f\mathrm{CO}_2$ decrease towards the Continental Water Boundary, where a maximum air-sea CO_2 disequilibrium ($-80\,\mu$atm) was reached at 61.9° S. This latitudinal band between the Polar Front and the Continental Water Boundary is characterized by the divergence of east and west wind belts (Klinck and Nowlin, 1986) that cause
the upwelling of the North Atlantic Deep Water. This surface input of iron-rich deep waters combined with strong stratification phases stimulated high rates of primary production (Legendre et al., 1992; Arrigo et al., 1997; Metzl et al., 1991; Poisson et al., 1994) that ultimately translated into the lowest $f\mathrm{CO}_2^{sw}$ values recorded in 2008. This conjecture is supported by the fact that the photosynthetic activity in the Antarctic Di-
vergence region significantly increased from 2007 to 2008, i.e., from $0.12\pm0.02\,\mathrm{mg\,m^{-3}}$ to $0.17\pm0.01\,\mathrm{mg\,m^{-3}}$. Thus, the ocean sequestration of CO_2 in 2008 exceeded that in 2007 ($-1.8\pm1.2\,\mathrm{mol\,m^{-2}\,yr^{-1}}$ and $-0.4\pm0.3\,\mathrm{mol\,m^{-2}\,yr^{-1}}$, respectively), as expected. Nevertheless, the highest uptake rates of CO_2 ($-6.5\,\mathrm{mol\,m^{-2}\,yr^{-1}}$) were reached due to the compensation of high WS of $15.4\,\mathrm{m\,s^{-1}}$ at 56.25° S, far from the area of largest
$\Delta f\mathrm{CO}_2$ undersaturation. On the other hand, the shelf waters of the Southern Ocean showed an onshore increase of $\Delta f\mathrm{CO}_2$ provoked by an intense growth of phytoplanktonic communities ($>0.30\,\mathrm{mg\,m^{-3}}$) located over the continental slope of the Livingston Island (Perissinotto et al., 1992, 2000; Pakhomov and Froneman, 1999; Blain et al., 2001). In summary, the distal shelf of the DP province acted as a slight source of
CO_2 to the atmosphere ($0.1\pm0.3\,\mathrm{mol\,m^{-2}\,yr^{-1}}$) while ocean waters displayed average annual uptake rates of $-1.1\pm0.9\,\mathrm{mol\,m^{-2}\,yr^{-1}}$.

3.3 Long-trends of biochemical variables

In order to gain consistency and reduce the long term variability registered during the successive FICARAM cruises, all highly heterogenic measurements gathered on the distal shelf were excluded in further analysis. Values of the Northwest Atlantic basin, which corresponded to measurements made during spring 2007 mainly in the CC province, were neither considered in this study due to the known existing differences with the Eastern basin (Lüger et al., 2004). Figure 3 graphically depicts the average values for each province of every variable measured during each FICARAM cruise (error bars stand for the respective standard deviation). The seasonal mean values were used to obtain a linear fit and thereby estimate significant ($p<0.05$) long-term trends so as to include them as well and complete the database. These interannual trends should only be taken into account as year-to-year trends of the respective seasons due to the seasonal interannual variability (Lefevre et al., 2004; Padin et al., 2008).

The northern provinces showed substantial changes at an annual scale for some of the variables. The interannual variability of SST and $\Delta f CO_2$ indicate a warming and increasing CO_2 saturation of surface waters in the Eastern North Atlantic (Fig. 3a, b). These general trends were observed under conditions of decreasing North Atlantic Oscillation index (NAO) (Osborn, 2007; González-Davila et al., 2007) that describes the influence of large-scale atmospheric pressure structures on warming and air-sea CO_2 disequilibrium of surface waters (Lüger et al., 2004; Omar and Olsen, 2006; Schuster and Watson, 2007). The freshening of surface waters was also evident, except in the case of the CC province, where this was not significant (Fig. 3b) due to the weakening of local mixing processes and shifts in northward advection of less saline waters (Santana-Casiano et al., 2007). A significant WS decrease of $-0.30\pm0.07\,\mathrm{m\,s^{-1}\,yr^{-1}}$ was appreciated during the spring cruises (Fig. 3b). Also during spring a long-term trend of chl-a ($-0.3\pm0.1\,\mathrm{mg\,m^{-3}\,yr^{-1}}$) revealed a reduction in the photosynthetic activity of oligotrophic waters in the NEC province (Fig. 4c).

Regarding southern provinces, the NECC showed a sustained interannual decrease

of SSS ($-0.16\pm0.01\,\mathrm{yr}^{-1}$) in its North Atlantic end during the autumn season provoked by an increase of rainfall rates and riverine inputs from the Amazon River (Fig. 3d). The freshening of these waters coincided with an outstanding $\Delta f\mathrm{CO}_2$ reduction ($-3.5\pm0.9\,\mu\mathrm{atm}\,\mathrm{yr}^{-1}$) and a consequent rise in the oceanic CO_2 uptake ($-0.09\pm0.03\,\mathrm{mol}\,\mathrm{m}^{-2}\,\mathrm{yr}^{-1}$). The fertilization of tropical surface waters from continental discharges seems to have stimulated the biological CO_2 drawdown (Lefevre et al., 1998), even though no significant response was detected in terms of chl-*a*. In any case, these observed interannual variability in the western basin of the NECC province backs up the influential role of the Amazon River plume in the uptake of CO_2 (Subramanian et al., 2008).

In the equatorial upwelling sector of the SEC province an interannual surface warming of $0.11\pm0.03°\mathrm{C}\,\mathrm{yr}^{-1}$ during the spring season was observed parallel to a WS decrease of $-0.58\pm0.14\,\mathrm{m}\,\mathrm{s}^{-1}\,\mathrm{yr}^{-1}$ that suggest weaker inputs of colder subsurface waters (Fig. 3e). In addition, coarsely trended drops in SSS, $\Delta f\mathrm{CO}_2$ and $F\mathrm{CO}_2$ were observed along the equator. Similarly, a decrease in the WS field of $-0.50\pm0.11\,\mathrm{m}\,\mathrm{s}^{-1}\,\mathrm{yr}^{-1}$ was also found of the SAS province (Fig. 3g), with maximum troughs of $-1.24\pm0.26\,\mathrm{m}\,\mathrm{s}^{-1}\,\mathrm{yr}^{-1}$ in the SAC region (Fig. 3h). Furthermore, several year-to-year changes envisaged in the Patagonian Sea (Fig. 3g, h, i) are expected to be of especial relevance in the convergence region of the Brazil and Falkland Currents, where the formation of Central Waters takes place (Fig. 3h).

3.4 Analysis of the biogeochemical forcing on the $f\mathrm{CO}_2^{\mathrm{sw}}$ variability

The $f\mathrm{CO}_2^{\mathrm{sw}}$ measurements gathered during the FICARAM cruises were modelled with an empirical algorithm according to their biogeochemical variability and geographical position, distinguishing ocean areas from shelf areas. Prior to making this multiple regression, all measurements were referenced to their respective months of year 2005, which was arbitrarily chosen as a reference year. This adjustment consisted in adding or subtracting to each sample the $x\mathrm{CO}_2^{\mathrm{atm}}$ difference between the corresponding mea-

surement date and the one in 2005. The effect of temperature on the $f\mathrm{CO}_2^{\mathrm{sw}}$ measurements was removed by normalising the observations to the mean in situ SST of the above-listed regions, after Takahashi et al. (1993). This new normalised and corrected variable ($'f\mathrm{CO}_2^{\mathrm{sw}}$) was finally used to obtain the aforementioned empirical algorithm, given in Eq. (4). Since the $'f\mathrm{CO}_2^{\mathrm{sw}}$ variability in each region was fitted from a single algorithm for both southward and northward cruises, a seasonal bias towards autumn conditions could be affecting our results, given the small amount of spring cruises available. The multiple linear regression coefficients were obtained using a forward stepwise method where only parameters that accounted for at least 1% of the $'f\mathrm{CO}_2^{\mathrm{sw}}$ variability were included in the algorithm.

$$'f\mathrm{CO}_2^{\mathrm{sw}} = A + B\,\mathrm{lon} + C\,\mathrm{lat} + D\,\mathrm{chl}{-}a + \sum_{i=1}^{3}\left(\varphi_i(\mathrm{SST}-\mu_{\mathrm{SST}})^i + \beta_i(\mathrm{SSS}-\mu_{\mathrm{SSS}})^i\right) \quad (4)$$

The μ_{SST} and μ_{SSS} stand for averages value of SST and SSS, respectively (Table 2). The regression coefficients for Eq. (4) and the percentage of $f\mathrm{CO}_2^{\mathrm{sw}}$ variability explained by each parameter in the different provinces are given in Table 3. Generally, SST is the parameter that determines most of the $f\mathrm{CO}_2^{\mathrm{sw}}$ variability, particularly in sub-tropical waters (>80% in the ENAS and STG provinces, with root mean square errors of $8\,\mu\mathrm{atm}$ and $13\,\mu\mathrm{atm}$, respectively), as shown previously (Lefevre and Taylor, 2002). On the contrary, in subtropical shelf regions the importance of the SST coefficient remained only true in the STG province, while in the distal shelf of the ENAS region the $f\mathrm{CO}_2^{\mathrm{sw}}$ variability explained by this factor drops down to 36%. This set forth the relevant role of the biological CO_2 drawdown factor, which showed an outstanding influence of 11% in the coastal $f\mathrm{CO}_2^{\mathrm{sw}}$ variability in this part of the North-West African upwelling system. Although the forcing of phytoplankton activity accounted only for 1% of the $f\mathrm{CO}_2^{\mathrm{sw}}$ variability, this was rather significant in ocean waters of the ENAS province, indicating the relevance of offshore influence from upwelling events (Hill et al., 1998).

In the tropical waters of the CC province SST was able to explain 69% of the $f\mathrm{CO}_2^{\mathrm{sw}}$ variability. A similar case applies to the NEC region but in this occasion the SSS gains

weight in Eq. (4), explaining 14% of the $f\text{CO}_2^{\text{sw}}$ variability. This rising dominance of SSS over the rest of the considered explanatory variables reaches its maximum in the southernmost waters of the NECC region. Here, SSS is able to account for 61% of the observed $f\text{CO}_2^{\text{sw}}$ variability, showing a clear direct relationship of 16.2±0.4 μatm

5   per SSS unit. This finding confirms the biological CO_2 uptake, largely dependant on the Amazon outflow (Muller-Karger et al., 1988) as the interannual analysis suggested. In the equatorial upwelling system the weight of SSS vanishes and SST variability comes to be again the main factor affecting $f\text{CO}_2^{\text{sw}}$ (58% of its variability explained) and shows the strongest SST-$\Delta f\text{CO}_2$ dependence (-22.2±0.3 μatm °C^{-1}) registered

10 during the FICARAM project. This exceptional correlation points towards the existence of a meridional distribution of different waters in the equatorial region, probably associated with the ventilation of upwelled subsurface waters.

Regarding the Southern Hemisphere, the observed $f\text{CO}_2^{\text{sw}}$ variability was poorly resolved by Eq. (4) compared to the northern provinces, likely due to a larger coastal in-

15 fluence. The observed heterogeneous $f\text{CO}_2^{\text{sw}}$ fields also handicapped an adequate description of these regions from the sole information gathered in surface layer sampling along the tracks of the ships, which often run closely from several frontal regions. Some remarkable differences between the in situ and modelled $f\text{CO}_2^{\text{sw}}$ values in the SAS and SAC provinces exceeded 20 μatm. The maximum discrepancies correspond to the

20 shelf and ocean regions of the FC province (28.9 and 31.0 μatm, respectively). The extremely complex and turbulent hydrographical conditions of the Southern Ocean make that non-linear interactions of the explanatory variables in Eq. (4), like SST^2 or SSS^2, gain importance over the rest in the Patagonian Sea. Similarly, the chl a distribution, which has an outstanding influence on the $f\text{CO}_2^{\text{sw}}$ in these regions, showed opposite

25 regression coefficients to the expected ones. The positive correlations found between $f\text{CO}_2^{\text{sw}}$-chl-a can be explained by some oceanographic processes of the Patagonian Sea (Bianchi et al., 2009), such as the intense $f\text{CO}_2^{\text{sw}}$ input from upwelling events and remineralization processes make the biological drawdown of CO_2 hardly noticeable (Perez et al., 1999). Furthermore, the enduring fingerprints of phytoplankton blooms

on the $f\text{CO}_2^{\text{sw}}$ signals could easily be held responsible for the positive regression coefficients throughout the entire non-synoptic sampling strategies followed in the FICARAM project.

On the southernmost waters of the DP province, the empirical algorithm obtained for computing autumn $f\text{CO}_2^{\text{sw}}$ measurements yielded an error of 11.1 μatm, in spite of the difficulties in reconstructing $f\text{CO}_2^{\text{sw}}$ in these waters from different methods (Metzl et al., 1995; Louanchi et al., 1996; Takahashi et al., 1997). The SST again played a key role in explaining 75% of the $f\text{CO}_2^{\text{sw}}$ variability, showing a high regression coefficient ($-21.2\pm0.3\,\mu\text{atm}\,^{\circ}\text{C}^{-1}$) similarly to the SEC region that is another well-known upwelling system, like the Southern Ocean. Regarding shelf waters, the $f\text{CO}_2^{\text{sw}}$ distribution only showed significant correlation with latitude, which acts as a proxy of the clearly observed biochemical changes under the coastal influence. With the exception of the latter result, geographical information had generally little importance in the different algorithms, suggesting that the selected provinces used to analyse the FICARAM dataset were rather well defined.

4 Summary

The FICARAM programme has proved to be an initiative of importance in collecting underway $f\text{CO}_2^{\text{sw}}$ measurements that covered an ample assort of hydrographic regions along the Atlantic Ocean over almost a decade. The obtained surface fields of $f\text{CO}_2^{\text{sw}}$ registered some general annual trends of the air-sea CO_2 exchanges in the Atlantic Ocean and, importantly, have allowed detecting some changes in the long-term trends of the fluxes and analysing the biogeochemical forcing of the $f\text{CO}_2^{\text{sw}}$ variability. The most remarkable results obtained are:

– The Northern Subtropical Gyre has acted as a sink of atmospheric CO_2 during the successive spring seasons ($-1.8\pm1.2\,\text{mol m}^{-2}\,\text{yr}^{-1}$) and as a source during autumn ($0.2\pm0.4\,\text{mol m}^{-2}\,\text{yr}^{-1}$). Similarly, the subtropical waters of the South-

Printer-friendly Version

Interactive Discussion

ern Hemisphere absorbed CO_2 under spring conditions (-0.2 ± 0.7 mol m^{-2} yr^{-1}), while CO_2 outgasing occurred during autumn (0.6 ± 0.6 mol m^{-2} yr^{-1}). The seasonal distribution of $f CO_2^{sw}$ in these latitudes was mainly determined by changes in SST that explained more than 80% of the $f CO_2^{sw}$ variability, according to the proposed algorithm.

– Tropical waters were virtually in equilibrium with the atmosphere during spring and autumn, which yielded trifling air-sea CO_2 fluxes, especially in the NECC region. The analysed property distributions in the latter province revealed a significant long-term decrease of SSS (-0.16 ± 0.01 yr^{-1}) during the boreal autumn, parallel to an outstanding $\Delta f CO_2$ reduction ($-3.5\pm0.9\,\mu$atm yr^{-1}) and its associated rise of oceanic CO_2 uptake (-0.09 ± 0.03 mol m^{-2} yr^{-1}). These strong SSS changes produced by the Amazon River outflows accounted for 61% of the observed $f CO_2^{sw}$ variability, providing uplift to the role of freshwater discharges in the uptake of CO_2.

– The equatorial upwelling system was highly supersaturated with CO_2 during the whole FICARAM project. This state eventually reached southern latitudes during the autumn season. An interannual surface warming of $0.11\pm0.03°$C yr^{-1} and a WS decrease of -0.58 ± 0.14 m s^{-1} yr^{-1} characterized these waters during the successive spring cruises, which suggests weaker inputs of colder subsurface waters.

– The majority of provinces in the Patagonian Sea behaved as an intense sink of CO_2 during autumn and spring, in particular the oceanic waters of the SAC province that were the strongest CO_2 sink (-5.4 ± 3.6 mol m^{-2} yr^{-1}) registered by the FICARAM cruises. The surface waters of the Patagonian shelf showed abrupt changes in the $\Delta f CO_2$ and $F CO_2$ distributions that could not be satisfactorily explained from either SST, SSS or chl-*a* due to the complex hydrography of the Southern Ocean.

BGD

6, 5589–5622, 2009

Air-sea CO_2 fluxes in the Atlantic

X. A. Padin et al.

Title Page	
Abstract	Introduction
Conclusions	References
Tables	Figures

◄◄	►►
◄	►
Back	Close

Full Screen / Esc

Printer-friendly Version

Interactive Discussion

– The Antarctic waters in the Drake Passage were found to be CO_2 undersaturated during the boreal autumn. They showed a clear southward decrease of $\Delta f CO_2$, towards the Continental Water Boundary. The oceanic waters of this region displayed an average uptake rate of $-1.1\pm0.9\,\mathrm{mol\,m^{-2}\,yr^{-1}}$, as opposed to those in the distal shelf, which acted as a slight source of CO_2 to the atmosphere $(0.1\pm0.3\,\mathrm{mol\,m^{-2}\,yr^{-1}})$.

References

Arrigo, K. R., Worthen, D., Lizotte, D. L., Dixon, P., and Dieckman, G.: Primary production in Antarctic sea ice, Science, 276, 394–397, 1997.

Bakun, A. and Parrish, R. H.: Comparative studies of coastal pelagic fish reproductive habitats: the anchovy (Engraulis anchoita) of the southwestern Atlantic, ICES J. Mar. Sci.: J. Conseil, 48, 343–361, 1991.

Barton, E. D.: Ocean Currents: Atlantic Eastern Boundary-Canary Current/Portugal Current, Encyclopedia of Ocean Sciences, edited by: Steele, J., Thorpe, S., and Turekian, K., Academic Press, London, 1, 380–389, 2001.

Battle, M., Bender, M. L., Tans, P. P., White, J. W. C., Ellis, J. T., Conway, T., and Francey, R. J.: Global carbon sinks and their variability inferred from atmospheric O_2 and delta C13, Science, 287, 2467–2470, 2000.

Bianchi, A. A., Giulivi, C. F., and Piola, A. R.: Mixing in the Brazil-Malvinas confluence, Deep-Sea Res. Pt. II, 40, 1345–1358, 1993.

Bianchi, A. A., Bianucci, L., Piola, A. R., Pino, D. R., Schloss, I., Poisson, A., and Balestrini, C.

F.: Vertical stratification and air-sea CO_2 fluxes in the Patagonian shelf, J. Geophys. Res.-Oceans, 110, C07003, doi:10.1029/2004JC002488, 2005.

Bianchi, A. A., Pino, D. R., Perlender, H. G. I., Osiroff, A. P., Segura, V., Lutz, V., Clara, M. L., Balestrini, C. F., and Piola, A. R.: Annual balance and seasonal variability of sea-air CO_2 fluxes in the Patagonia Sea: Their relationship with fronts and chlorophyll distribution, J. Geophys. Res.-Oceans, 114, C03018, doi:10.1029/2008JC004854, 2009.

Blain, S., Tréguer, P., Belviso, S., Bucciarelli, E., Denis, M., Desabre, S., Fiala, M., Martin Jézéquel, V., Le Fèvre, J., and Mayzaud, P.: A biogeochemical study of the island mass effect in the context of the iron hypothesis: Kerguelen Islands, Southern Ocean, Deep-Sea Res. Pt. I, 48, 163–187, 2001.

Canadell, J. G., Le Quéré, C., Raupach, M. R., Field, C. B., Buitenhuis, E. T., Ciais, P., Conway, T. J., Gillett, N. P., Houghton, R. A., and Marland, G.: Contributions to accelerating atmospheric CO_2 growth from economic activity, carbon intensity, and efficiency of natural sinks, P. Natl. Acad. Sci. USA, 104, 10288–10293, 2007.

Chen, C. T. A. and Borges, A. V.: Reconciling opposing views on carbon cycling in the coastal ocean: Continental shelves as sinks and near-shore ecosystems as sources of atmospheric CO_2, Deep-Sea Res. Pt. II, doi:10.1016/j.dsr2.2009.01.001, 2009.

DOE: Handbook of methods for the analysis of various parameters of carbon dioxide in seawater (version 2), 1994.

Emery, W. J. and Dewar, J. S.: Mean temperature-salinity, salinity-depth and temperature-depth curves for the North Atlantic and the North Pacific, Prog. Oceanogr., 11, 219–305, 1982.

Francey, R. J., Tans, P. P., Allison, C. E., Enting, I. G., White, J. W. C., and Trolier, M.: Changes in oceanic and terrestrial carbon uptake since 1982, Nature, 373, 326–330, 1995.

Froneman, P. W., McQuaid, C. D., and Laubscher, R. K.: Size-fractionated primary production sudies in the vicinity of the Subtropical Front and an adjacent warm-core south of Africa in austral winter, J. Plankton Res., 21, 2019–2035, 1999.

González-Dávila, M., Santana-Casiano, J. M., and González-Dávila, E. F.: Interannual variability of the upper ocean carbon cycle in the northeast Atlantic Ocean, Geophys. Res. Lett., 34, L07608, doi:10.1029/2006GL028145, 2007.

Gordon, A. L.: Brazil-Malvinas confluence-1984, Deep-Sea Res. Pt. II, 36, 359–384, 1989.

Guerrero, R., Acha, E., Framinan, M., and Lasta, C.: Physical oceanography of the River Plate Estuary, Argentina, Cont. Shelf Res., 17, 727–742, 1997.

Hill, A. D., Hickey, B. M., Shillington, F. A., Strub, P. T., Brink, K. H., Barton, E., and Thomas, A.

C.: Eastern ocean boundaries, Coastal segment (E), The Sea, 11, 29–65, 1998.

Hooker, S. B., Rees, N. W., and Aiken, J.: An objective methodology for identifying oceanic provinces, Prog. Oceanogr., 45, 313–338, 2000.

Hooker, S. B., Esaias, W. E., Feldman, G. C., Gregg, W. W., and McClain, C. R.: An overview of SeaWiFS and ocean colour, in: NASA Technical Memo 104566, edited by: Hooker, S. B. and Firestone, E. R., vol. 1, NASA Goddard Space, Flight Centre, Greenbelt, MA, 1, 24 1992.

Houghton, R. A.: Revised estimates of the annual net flux of carbon to the atmosphere from changes in land use and land management 1850–2000, Tellus B, 55, 378–390, doi:10.1034/j.1600-0889.2003.01450.x, 2003.

Kalnay, E., Kanamitsu, M., Kistler, R., Collins, W., Deaven, D., Gandin, L., Iredell, M., Saha, S., White, G., and Woollen, J.: The NCEP/NCAR reanalysis project, B. Am. Meteorol. Soc., 77, 437–471, 1996.

Keeling, C. D.: Carbon dioxide in surface ocean waters, 4. Global distribution, J. Geophys. Res., 73, 4543–4553, 1968.

Keeling, C. D., Whorf, T. P., Wahlen, M., and Plicht, J.: Interannual extremes in the rate of rise of atmospheric carbon dioxide since 1980, Nature, 375, 666–670, 1995.

Keeling, C. D. and Whorf, T. P.: The 1800-year oceanic tidal cycle: A possible cause of rapid climate change, P. Natl. Acad. Sci. USA, 97(10), 3814–3819, 2000.

Körtzinger, A., Thomas, H., Schneider, B., Gronau, N., Mintrop, L., and Duinker, J. C.: At-sea intercomparison of two newly designed underway pCO_2 systems – encouraging results, Mar. Chem., 52, 133–145, 1996.

Lefevre, N., Moore, G., Aiken, J., Watson, A., Cooper, D., and Ling, R.: Variability of pCO_2 in the tropical Atlantic in 1995, J. Geophys. Res., 103, 5623–5634, 1998.

Lefevre, N. and Taylor, A.: Estimating pCO_2 from sea surface temperatures in the Atlantic gyres, Deep Sea Res. Pt. I, 49, 539–554, 2002.

Lefèvre, N., Watson, A. J., Olsen, A., Ríos, A. F., Pérez, F. F., and Johannessen, T.: A decrease in the sink for atmospheric CO_2 in the North Atlantic, Geophys. Res. Lett, 31, L07306, doi:10.1029/2003GL018957, 2004.

Legendre, L., Ackley, S. F., Dieckmann, G. S., Gulliksen, B., Horner, R., Hoshiai, T., Melnikov, I. A., Reeburgh, W. S., Spindler, M., and Sullivan, C. W.: Ecology of sea ice biota, Polar Biol., 12, 429–444, 1992.

Longhurst, A., Sathyendranath, S., Platt, T., and Caverhill, C.: An estimate of global primary

Air-sea CO_2 fluxes in the Atlantic

X. A. Padin et al.

production in the ocean from satellite radiometer data, J. Plankton Res., 17, 1245–1271, 1995.

Louanchi, F., Mtzl, N., and Poisson, A.: Modelling the surface fCO_2 fields in the Indian ocean, Mar. Chem., 55, 265–279, 1996.

5 Luger, H., Wallace, D. W. R., Kortzinger, A., and Nojiri, Y.: The pCO_2 variability in the midlatitude North Atlantic Ocean during a full annual cycle, Global Biogeochem. Cy., 18(3), GB3023, doi:10.1029/2003GB002200, 2004.

Metzl, N., Beauverger, C., Brunet, C., Goyet, C., and Poisson, A.: Surface water carbon dioxide in the southwest Indian sector of the Southern Ocean: a highly variable CO_2 source/sink

10 region in summer, Mar. Chem., 35, 85–95, 1991.

Metzl, N., Tilbrook, B., and Poisson, A.: The annual fCO_2 cycle and the air-sea CO_2 flux in the sub-Antarctic Ocean, Tellus B, 51, 849–861, 1999.

Metzl, N.: Air-sea CO_2 fluxes in the Southern Ocean: natural and methodological variabilities, SOLAS Open Conference, Halifax, 13–16 October, 2004.

15 Metzl, N., Poisson, A., Louanchi, F., Brunet, C., Schauer, B., and Bres, B.: Spatio-temporal distributions of air-sea fluxes of CO_2 in the Indian and Antarctic oceans, Tellus, 47B, 56–99, 1995.

Mittelstaedt, E.: The ocean boundary along the northwest African coast: circulation and oceanographic properties at the sea surface, Prog. Oceanogr., 26, 307–355, 1991.

20 Muller-Karger, F. E., McClain, C. R., and Richardson, P. L.: The dispersal of the Amazon's water, Nature, 333, 56–59, 1988.

Nowlin Jr., W. D. and Klinck, J. M.: The physics of the Antarctic Circumpolar Current, Geophys. Res. Lett, 24, 469–491, 1986.

Olsen, A., Trinanes, J. A., and Wanninkhof, R.: Sea-air flux of CO_2 in the Caribbean Sea

25 estimated using in situ and remote sensing data, Remote Sens. Environ., 89, 309–325, 2004.

Omar, A. M. and Olsen, A.: Reconstructing the time history of the air-sea CO_2 disequilibrium and its rate of change in the eastern subpolar North Atlantic, 1972–1989, Geophys. Res. Lett, 33, L04602, doi:10.1029/2005GL025425, 2006.

30 Osborn, T.: North Atlantic Oscillation index data, http://www.cru.uea.ac.uk/~timo/projpages/ nao_update.htm, 2007.

Padin, X. A., Vázquez-Rodríguez, M., Rios, A. F., and Pérez, F. F.: Atmospheric CO_2 measurements and error analysis on seasonal air-sea CO_2 fluxes in the Bay of Biscay, J. Marine

Air-sea CO_2 fluxes in the Atlantic

X. A. Padin et al.

Syst., 66, 285–296, doi:10.1016/j.jmarsys.2006.05.010, 2007.

Padin, X. A., Castro, C. G., Ríos, A. F., and Pérez, F. F.: fCO$_2$sw variability in the Bay of Biscay during ECO cruises, Cont. Shelf Res., 28, 904–914, 2008.

Pérez, F. F., Ríos, A. F., and Rosón, G.: Sea surface carbon dioxide off the Iberian peninsula (North Eastern Atlantic Ocean), J. Marine Syst., 19, 27–46, 1999.

Perissinotto, R., Laubscher, R. K., and McQuaid, C. D.: Marine productivity enhancement around Bouvet and the South Sandwich Islands (Southern Ocean), Mar. Ecol.-Prog. Ser., 88, 41–53, 1992.

Perissinotto, R., Lutjeharms, J. R. E., and van Ballegooyen, R. C.: Biological-physical interactions and pelagic productivity at the Prince Edward Island, Southern Ocean, J. Marine Syst., 24, 327–341, 2000.

Piola, A. R. and Rivas, A. L.: Antecedentes históricos de las exploraciones en el mar y las características ambientales, Corrientes en la Plataforma Continental, in: El Mar Argentino y sus Recursos Pesqueros, edited by: Boschi, E. E., Instituto Nacional de Investigación y Desarrollo Pesquero, Mar del Plata, 1, 119–132, 1997.

Poisson, A., Metzl, N., Brunet, C., Schauer, B., Bres, B., Ruíz-Pino, D., and Louanchi, F.: Variability of sources and sinks of CO$_2$ in the Western Indian and Southern Oceans during the year 1991, J. Geophys. Res., 98, 22759–22778, 1993.

Ríos, A. F., Pérez, F. F., and Fraga, F.: Water masses in the upper and middle North Atlantic Ocean east of the Azores, Deep-Sea Res. Pt. II, 39, 645–658, 1992.

Sabine, C. L., Feely, R. A., Gruber, N., Key, R. M., Lee, K., Bullister, J. L., Wanninkhof, R., Wong, C. S., Wallace, D. W. R., Tilbrook, B., Millero, F. J., Peng, T. H., Kozyr, A., Ono, T., and Ríos, A. F.: The oceanic sink for anthropogenic CO$_2$, Science, 305, 5682, 367–371, 2004.

Santana-Casiano, J. M., González-Dávila, M., Rueda, M. J., Llinás, O., and González-Dávila, E. F.: The interannual variability of oceanic CO$_2$ parameters in the northeast Atlantic subtropical gyre at the ESTOC site, Global Biogeochem. Cy., 21, GB1015, doi:10.1029/2006GB002788, 2007.

Sarmiento, J. L. and Gruber, N.: Sinks for anthropogenic carbon, Phys. Today, 55, 30–36, 2002.

Schuster, U. and Watson, A. J.: A variable and decreasing sink for atmospheric CO$_2$ in the North Atlantic, J. Geophys. Res, 112, C11006, doi:10.1029/2006JC003941, 2007.

Siegenthaler, U. and Sarmiento, J. L.: Atmospheric carbon dioxide and the ocean, Nature, 365, 119–125, 1993.

Air-sea CO$_2$ fluxes in the Atlantic

X. A. Padin et al.

Subramaniam, A., Yager, P. L., Carpenter, E. J., Mahaffey, C., Björkman, K., Cooley, S., Kustka, A. B., Montoya, J. P., Sañudo-Wilhelmy, S. A., and Shipe, R.: From the Cover: Amazon River enhances diazotrophy and carbon sequestration in the tropical North Atlantic Ocean, P. Natl. Acad. Sci. USA, 105, 10460–10465, 2008.

5 Takahashi, T.: Carbon dioxide in the atmosphere and in Atlantic ocean water, J. Geophys. Res., 66, 477–494, 1961.

Takahashi, T., Olafsson, J., Goddard, J. G., Chipman, D. W., and Sutherland, S. C.: Seasonal variation of CO_2 and nutrients in the high-latitude surface oceans: a comparative study, Global Biogeochem. Cy., 7, 843–878, 1993.

10 Takahashi, T., Feely, R. A., Weiss, R. F., Wanninkhof, R. H., Chipman, D. W., Surherland, S. C., and Takahashi, T. T.: Global air-sea flux of CO_2: An estimate based on measurements of sea-air pCO_2 difference, P. Natl. Acad. Sci. USA, 94, 8292–8299, 1997.

Takahashi, T., Sutherland, S. C., Wanninkhof, R., Sweeney, C., Feely, R. A., Chipman, D. W., Hales, B., Friederich, G., Chavez, F., Sabine, C., Watson, A. J., Bakker, D. C., Schuster, U.,

15 Metzl, N., Yoshikawa-Inoue, H., Ishii, M., Midorikawa, T., Nojiri, Y., Körtzinger, A., Steinhoff, T., Hoppema, M., Olafsson, J., Arnarson, T. S., Tilbrook, B., Johannessen, T., Olsen, A., Bellerby, R., Wong, C. S., Delille, B., Bates, N. R., and de Baar, H. J. W.: Climatological mean and decadal change in surface ocean pCO_2, and net sea-air CO_2 flux over the global oceans, Deep-Sea Res. Pt. II, doi:10.1016/j.dsr2.2008.12.009, 2008.

20 Thomas, H., Bozec, Y., Elkalay, K., and De Baar, H. J. W.: Enhanced open ocean storage of CO_2 from shelf sea pumping, in: American Association for the Advancement of Science, 304, no. 5673, 1005–1008, 2004.

Trenberth, K. E., Large, W. G., and Olson, J. G.: The mean annual cycle in global ocean wind stress, J. Phys. Oceanogr., 20, 1742–1760, 1990.

25 Wanninkhof, R.: Relationship between wind speed and gas exchange over the ocean, J. Geophys. Res., 97, 7373–7382, 1992.

Weiss, R. F.: Carbon dioxide in water and seawater: the solubility of non-ideal gas, Mar. Chem., 2, 203–215, 1974.

Air-sea CO$_2$ fluxes in the Atlantic

X. A. Padin et al.

Table 1. Information of the FICARAM cruises.

Cruise	Ship	Date	Latitude range
FICARAM 1	B/O Hespérides	Oct–Nov 2000	36.5° N–11.1° S
FICARAM 2	B/O Hespérides	Mar–Apr 2001	40° N–55.1° S
FICARAM 3	B/O Hespérides	Oct–Nov 2001	36.6° N–7.8° S
FICARAM 4	B/O Hespérides	Mar–Apr 2002	36.0° N–51.0° S
FICARAM 5	B/O Hespérides	Oct–Nov 2002	37.4° N–23.1° S
FICARAM 6	B/O Hespérides	Apr 2003	37.1° N–19.1° N
FICARAM 7	B/O Hespérides	Oct–Nov 2004	37.3° N–55.1° S
FICARAM 8	B/O Hespérides	Oct–Nov, 2005	36.4° N–53.2° S
FICARAM 9	B/O Hespérides	Mar–Apr 2006	32.4° N–55.1° S
FICARAM 10	B/O Las Palmas	Oct–Nov 2006	37.4° N–53.2° S
FICARAM 11	B/O Las Palmas	Mar–May 2007	37.5° N–54.8° S
FICARAM 12	B/O Las Palmas	Oct–Nov 2007	36.0° N–62.9° S
FICARAM 13	B/O Las Palmas	Mar–Apr 2008	37.4° N–55.1° S
FICARAM 14	B/O Las Palmas	Oct–Nov 2008	37.5° N–62.9° S

Table 2. Statistics for the selected provinces on the different boreal seasons (spring; autumn) and areas (shelf; ocean): mean and standard deviation ($\mu \pm \sigma$) of SST, SSS, chl-a, $\Delta f CO_2$, WS, $F CO_2$.

Region	Boreal Season	Area	SST °C	SSS	chl-a mg m^{-3}	$\Delta f CO_2$ µatm	WS m s^{-1}	$F CO_2$ mol m^{-2} yr^{-1}
ENAS 39–27° N	*spring*	*shelf*	*18.1±0.2*	*36.4±0.0*	*0.04±0.00*	*−43±1*	*6.9±0.7*	*−2.0±0.0*
		ocean	***18.6±0.9***	***36.6±0.2***	***0.11±0.07***	***−34±12***	***7.4±2.5***	***−1.8±1.2***
	autumn	shelf	22.0±0.6	36.5±0.2	0.15±0.06	2±11	5.3±4.2	0.3±0.6
		ocean	**22.9±1.1**	**36.7±0.2**	**0.14±0.12**	**9±13**	**5.2±2.7**	**0.2±0.4**
CC 27–16° N	*spring*	*shelf*	*18.4±0.2*	*36.3±0.1*	*0.11±0.01*		*6.8±1.0*	
		ocean	***21.3±1.1***	***36.6±0.5***	***0.13±0.09***	***−19±13***	***8.9±1.4***	***−1.4±1.0***
	autumn	ocean	25.3±1.5	36.7±0.4	0.12±0.06	16±13	6.6±2.6	0.6±0.5
NEC 16–8° N	*spring*		***24.9±1.3***	***35.9±0.2***	***0.13±0.07***	***−17±10***	***7.6±1.8***	***−0.7±0.4***
	autumn	ocean	28.1±0.6	35.7±0.4	0.12±0.06	2±14	6.1±2.0	0.0±0.5
NECC 8–1° N	*spring*		***28.1±0.5***	***35.6±0.3***	***0.14±0.08***	***1±16***	***5.5±1.7***	***0.1±0.4***
	autumn	ocean	28.2±0.6	35.1±0.5	0.11±0.04	3±13	4.5±1.8	0.1±0.3
SEC 1° N–15° S	*spring*	*shelf*	*29.1±0.3*	*37.0±0.2*	*0.17±0.01*		*2.0±0.2*	
		ocean	***28.7±0.3***	***36.3±0.6***	***0.18±0.08***	***30±11***	***4.2±2.0***	***0.7±0.5***
	autumn	shelf	27.1±0.3	36.5±0.2	0.16±0.04	34±8	7.1±1.1	1.6±0.6
		ocean	**26.8±0.5**	**36.3±0.3**	**0.14±0.05**	**24±12**	**7.0±1.6**	**1.0±0.7**
STG 15–31° S	*spring*	*shelf*	*26.3±1.5*	*36.4±0.5*	*0.15±0.05*	*17±17*	*5.0±1.5*	*0.4±0.4*
		ocean	***27.4±1.0***	***36.9±0.3***	***0.17±0.06***	***21±14***	***5.8±1.9***	***0.6±0.6***
	autumn	shelf	23.8±1.5	36.5±0.5	0.13±0.02	14±9	8.6±3.2	0.5±0.7
		ocean	**23.9±1.7**	**36.8±0.4**	**0.17±0.07**	**−5±17**	**6.9±1.7**	**−0.2±0.7**
SAS 31–40° S	*spring*	*shelf*	*22.1±2.0*	*33.2±2.2*	*0.28±0.16*	*−19±27*	*5.4±2.7*	*−0.7±1.3*
		ocean	***20.7±4.1***	***35.0±1.1***	***0.24±0.10***	***−28±30***	***6.1±2.8***	***−0.9±1.5***
	autumn	shelf	14.9±2.5	32.6±1.1	0.18±0.09	−67±37	7.4±2.2	−3.2±2.7
		ocean	**17.8±1.8**	**35.6±0.5**	**0.11±0.04**	**−41±16**	**7.1±3.1**	**−2.2±2.1**
SAC 40–51° S	*spring*	*shelf*	*10.4±0.6*	*33.6±0.1*	*0.26±0.05*	*−42±9*	*9.0±1.1*	*−3.2±1.1*
		ocean	***11.9±2.2***	***34.0±0.2***	***0.26±0.10***	***−39±16***	***7.4±3.8***	***−1.9±2.1***
	autumn	shelf	9.5±2.1	33.4±0.3	0.11±0.03	−70±42	8.2±3.4	−4.1±4.0
		ocean	**9.3±1.4**	**33.8±0.1**	**0.15±0.06**	**−57±26**	**9.9±3.1**	**−5.4±3.6**
FC 51–56° S	*spring*	*shelf*	*9.2±0.6*	*33.3±0.3*	*0.40±0.15*	*−7±23*	*10.8±4.8*	*−0.7±2.8*
		ocean	***8.8±0.5***	***33.6±0.2***	***0.43±0.22***	***1±26***	***10.6±5.3***	***1.2±2.5***
	autumn	shelf	6.6±0.8	32.9±0.5	0.09±0.04	−15±32	10.4±3.0	−1.4±3.2
		ocean	**6.8±1.1**	**33.6±0.4**	**0.08±0.02**	**−50±40**	**9.7±3.5**	**−2.8±2.5**
DP 56–66° S	autumn	shelf	−0.8±0.7	34.1±0.1	0.14±0.05	8±14	3.9±1.6	0.1±0.3
		ocean	**1.3±2.3**	**33.8±0.2**	**0.10±003**	**−20±11**	**6.8±3.0**	**−1.1±0.9**

Air-sea CO_2 fluxes in the Atlantic

X. A. Padin et al.

Table 3. Regression coefficients (in italics) and variability explained (bold-faced) by each of the parameters included in the empirical algorithm given in Eq. (4) applied in every biogeochemical province where $fCO_2{}^{sw}{}_0$ mean the start point. The root mean square (rms), percentage of the explained variability by each parameter ($r^{2'}$) and the correlation coefficient (r^2) are also given. The "n" value stands for the number of valid data included in each analysis.

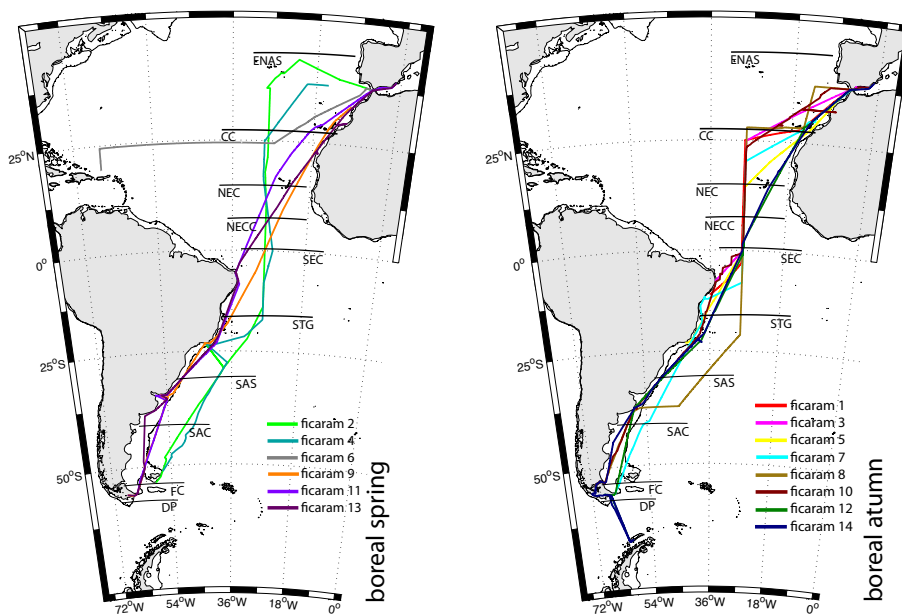| Region	area	rms r^2	$fCO_2{}^{sw}{}_0$ n	lon (°E)	lat (°N)	depth (m)	sst-μ (°C)	(sst-μ)² (°C²) $r^{2'}$	(sst-μ)³ (°C³)	sss-μ	(sss-μ)²	(sss-μ)³	chl-a (mg m⁻³)
ENAS 39–27°N	shelf	3.4 70	−634±190 109	−20±4 2	23±5 9	−0.04±0.01 6	−8.6±1.9 2	−3.6±0.7 4	1.3±0.5 30	*	60±16 4	−26±7 2	−3.8±1.4 11
	ocean	8.0 84	325±1 8498	*	1.33±0.03 *	* 4	−6.78±0.04 80	*	*	*	*	*	−3.9±0.2 1
CC 27–16°N	ocean	14 73	353±2 7970	0.70±0.04 1	1.4±0.1 3	*	−8.7±0.1 69	*	*	*	*	*	*
NEC 16–8°N	ocean	9.5 82	331±1 3734	*	*	*	−10.1±0.1 66	1.38±0.06 2	*	23.4±0.4 14	*	*	*
NECC 8–1°N	ocean	9.9 77	258±4 4116	−3.9±0.2 4	−2.18±0.08 7	*	−9.4±0.3 5	*	*	16.2±0.4 61	*	*	*
SEC 1°N–15°S	ocean	11.4 68	444±2 7755	1.69±0.06 10	0.72±0.04 1	*	−22.2±0.3 56	*	2.1±0.1 2	*	*	*	*
STG 15–31°S	shelf	12.3 87	456±5 860	*	2.4±0.2 2	0.07±0.02 4	−15.0±0.2 80	*	*	−12.4±1.0 1	*	*	*
	ocean	13.0 85	403±1 7376	1.90±0.04 3	−2.19±0.05 4	*	−12.2±0.1 77	*	−0.54±0.02 1	*	*	*	*
SAS 31–40°S	shelf	24.4 63	−856 1532	−58.3±2.2 11	55.0±2.2 3	−0.22±0.02 2	−5.9±0.3 43	−0.77±0.05 3	*	*	*	*	33.3±4.9 1
	ocean	11.7 89	425±2 2665	1.95±0.05 6	*	*	−10.1±0.1 78	0.76±0.02 4	*	−0.07±0.00 1	*	*	*
SAC 40–51°S	shelf	16.9 89	−889±25 1697	−23.4±0.5 6	3.5±0.2 1	*	6.8±0.1 74	*	*	164±4 8	*	*	*
	ocean	26.1 71	581±14 1847	*	5.4±0.3 2	*	−19.2±0.4 60	*	0.04±0.00 1	76±4 4	−101±7 3	*	38±4 1
FC 51–56°S	shelf	28.9 54	−310±51 1038	−10.0±0.8 2	*	*	−15.1±1.1 24	7.0±0.8 4	*	*	−23±2 11	−3.6±0.4 3	48±3 10
	ocean	31.0 61	−589±59 774	−14.2±0.9 8	*	0.03±0.00 4	−15.3±1.7 6	6.5±0.9 23	*	*	−34±4 4	−7.0±1.3 2	142±6 14
DP 56–66°S	shelf	4.0 93	−664.4 175	*	−16.9±0.3 93	*	*	*	*	*	*	*	*
	ocean	11.1 90	908±23 1413	*	8.9±0.4 3	0.01±0.00 1	−21.2±0.3 75	*	*	*	−189±6 11	*	*

Fig. 1. Map showing the ship tracks and biogeochemical provinces selected for the FICARAM cruises. Left panel gives boreal spring tracks and right panel the boreal autumn ones.
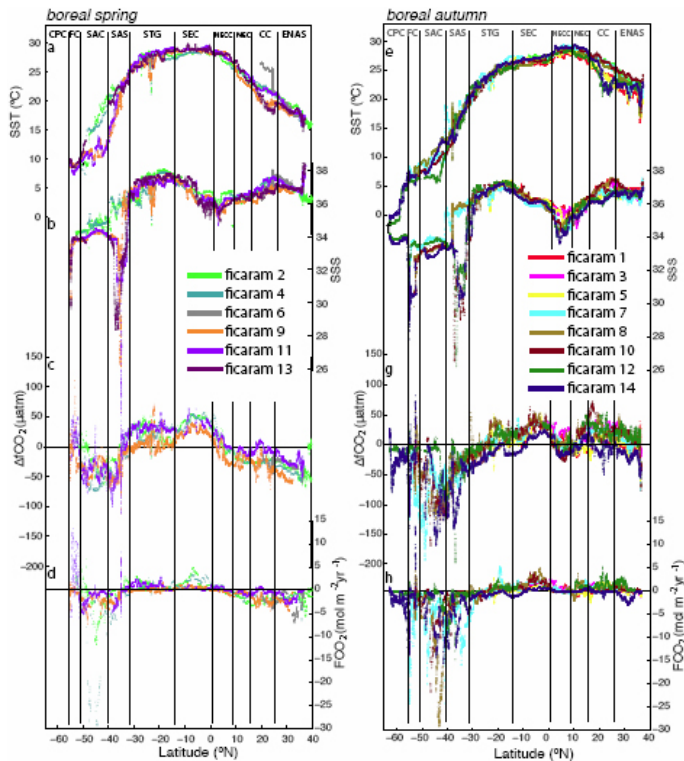
Fig. 2. Latitudinal distributions during boreal springs **(a–d)** and boreal autumns **(e–f)** of SST, SSS, $\Delta f\mathrm{CO}_2$ and computed $F\mathrm{CO}_2$ as measured in the FICARAM cruises.
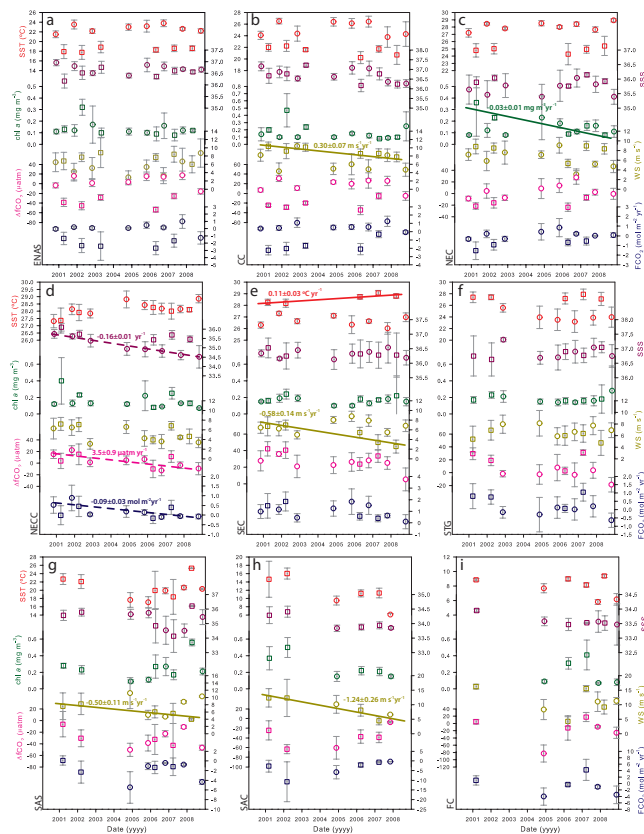
Printer-friendly Version

Interactive Discussion

Fig. 3. Temporal variation of the averaged SST, SSS, chl-*a*, WS, $\Delta f CO_2$ and $F CO_2$ cruise (error bars stand for the respective standard deviation) in each of the selected biogeochemical provinces. Spring and autumn values are shown as squares and circles, respectively. Significant regression lines ($p<0.05$) and regression slopes including the standard error are also given. Solid lines stand for spring results and dashed lines for autumn.